Thin–Walled Structures 202 (2024) 112120

Contents lists available at ScienceDirect

Thin-Walled Structures

journal homepage: www.elsevier.com/locate/tws

Full length article

Design of multi-stable metamaterial cell with improved and programmable energy trapping ability based on frame reinforced curved beams

Xiao Ju [a], Shaoqi Li [a,*], Yu Zhang [a], Penghao Wu [a], Yancheng Li [a,b]

[a] Centre for Innovative Structures, College of Civil Engineering, Nanjing Tech University, Nanjing 211816, China
[b] School of Civil and Environmental Engineering, University of Technology Sydney, Ultimo, NSW 2007, Australia

ARTICLE INFO

Keywords:
Negative stiffness
Energy trapping
Programmable metamaterial
Multi-stable

ABSTRACT

Curved beams are a class of elements capable of bi-stability and can be used to construct multi-stable metamaterials. These materials leverage elastic snap-through in curved beams to transition between multiple stable states, effectively achieving energy absorption and trapping. The elastic deformation allows the structure to be used repetitively. However, the conventional curved beam unit cells design process omits the influence of supporting frames, resulting in inadequate constrains of the beam in the fabricated metamaterials. Its mechanical properties and number of stable states can be significantly diverged from theoretical predictions. This paper presents a novel multi-stable metamaterial with improved and consistent energy trapping ability based on frame reinforced curved beams. Comparative finite element analysis of three unit-cell types demonstrates the superior bi-stability of the proposed cell. Moreover, parametric analysis reveals the proposed cell has a wider range of parameters that can achieve bi-stability. The mechanical properties of the single cell and the 2×2 metamaterial are obtained by compression tests. The results validate the linear mechanical response that correlates with the number of unit cells which allows optimal programming of multi-stable metamaterials. Finally, plate impact test is conducted to investigate and analyze the cushioning performance of the multi-stable metamaterial.

1. Introduction

Mechanical metamaterials [1,2], a specialized class of artificial materials, exhibit unique and extreme mechanical characteristics through the rational design of the unit cells [3–5]. Negative stiffness (NS) metamaterials are a promising type of mechanical metamaterials [6–8], exhibiting NS behavior which means the increase in deformation leads to a decrease in reaction force [9]. The unique properties of NS metamaterial unlock extensive potential across various fields, including vibration control [10,11], repeatable energy absorption and dissipation [12–14], shock isolation[15,16] and wave propagation control [17,18]. Although many NS metamaterials have been proposed and studied [19,20], the limitations of NS metamaterials have also been discovered in the research, such as the inability to dissipate energy quickly and avoid secondary impact. On this basis, multi-stable metamaterial [21,22], a special subclass of NS metamaterial, is proposed to solve this research dilemma.

Multi-stable metamaterials are a type of metamaterial that exhibits multiple stable states and are usually composed of bi-stable cells. The transition between different stable states is achieved through snap-through behavior [23], which possesses NS and offers high energy absorption without plastic deformation. The difference between normal mono-stable NS cell and bi-stable NS cell is that the valley force of the bi-stable cell is negative, as illustrated in Fig. 1(a) and (b). Negative valley force indicates that the structure not only absorbs energy but also releases a small amount of energy during deformation [22], presenting a local minimum in the energy-displacement curve as shown in Fig. 1(c) which implies that if no external energy is applied after finishing deformation, the deformation of the unit cell will remain. Thus, the energy corresponding to the bi-stable point is trapped by the structure in the form of elastic strain energy, and its value is equal to the energy absorbed by the structure minus the energy released. This energy trapping effect of the multi-stable structure is achieved through the switching between different stable states, relying on elastic instability which allows for repeated uses. Furthermore, this energy absorption mechanism has been proven independent of the loading rate and is solely related to the deformed and original shapes [24]. Additionally, the energy-locking effect of multi-stable metamaterials reduces or eliminates the rebound effect during impact, preventing the secondary damage caused by impact rebound [25].

* Corresponding author.
E-mail address: shaoqi@njtech.edu.cn (S. Li).

https://doi.org/10.1016/j.tws.2024.112120
Received 27 February 2024; Received in revised form 19 May 2024; Accepted 10 June 2024
Available online 19 June 2024

Due to its excellent properties and great potential, scholars have conducted extensive research on multi-stable metamaterials. Qiu et al. [26] proposed a type of curved beam and analyzed parameters required to achieve bi-stability through theoretical calculations as the reference principle for designing multi-stable metamaterials. Shan et al. [22] designed a class of metamaterials using tilted beam as bi-stable element, and investigated the influence of beam length and tilt angle on the bi-stable properties. The experiment showed that the proposed metamaterial structure exhibited intended multi-stability and made an order of about 80 % reduction in peak acceleration during impact. Ma et al. [25] designed a class of multi-stable auxetic metamaterials with the shuriken-shaped and the triangle unit cell and verified the energy dissipation and auxetic behavior by numerical simulation and experiments.

To improve the mechanical properties of the multi-stable metamaterials [27], scholars have implemented several strategies, such as using of different raw materials[28], the development of innovative metamaterial structural designs [29,30], and programmable design [31]. Zhang et al. [32]. proposed the lattice-based and hollow cross-section design of curved beams for multi-stable meta-structures. Experiment testing indicated that tuning the bending stiffness of unit cells while maintaining constant volume, can improve the mechanical properties of structures, including critical forces, energy dissipation, and impact performance. Wang et al. [33]. propose a programmable multi-stable metamaterial with tunable Poisson's ratio and band gap and demonstrate that it is suitable for a wide range of operating conditions in the field of vibration control. Liang et al. [34]. realized the precise programming of the snap-through sequence and deformation model by controlling the peak force of multi-stable metamaterial using the topology optimization method. Although several excellent functions, such as programmability, are introduced, most research on programmable multi-stable metamaterials focuses on programming the mechanical properties of unit cells. Programming the metamaterial properties based on the properties of the unit cells is studied rarely, and these researches tend to realize programmability by the dispersed arrangement of unit cells, which increases the volume and space occupancy of metamaterials.

In this work, a novel frame reinforced (FR) unit cell is proposed inspired by curved beam honeycomb unit cell design [35]. The mechanical response of several single cells under compression is compared by finite element analysis, and the effect of curved beam parameters on its mechanical properties is obtained by parametric analysis. In addition, the quasi-static compression experiments of the novel FR cell and the 2×2 metamaterial are conducted to verify the finite element analysis results and programmable properties. Finally, the cushion performance of multi-stable metamaterials is investigated by plate impact tests. The cushioning properties of multi-stable metamaterials are analyzed and explained through the presence of peak force and the energy trapping mechanism inherent in multi-stable behavior.

2. Structural design

2.1. Bi-stable curved beam

To realize a multi-stable metamaterial, the metamaterial unit cell needs to possess bi-stability. This study chooses the sinusoidal curved beam as the bi-stable element. The shape of the curved beam is determined by the first mode of buckling of a straight beam, as presented in Fig. 2(a). The geometric parameters of the curved beam are defined as follows: the beam thickness t, the length l, the curved beam height h, and the depth b. The geometry of the curved beam, $\omega(x)$, can be described as follows:

$$\omega(x) = \frac{1}{2}h\left[1 - sin\left(\frac{\pi}{2} - 2\pi\frac{x}{l}\right)\right] \quad (1)$$

When a vertically downward force f is applied at the center, the curved beam undergoes buckling deformation, enabling it to achieve bi-stability. In this process, the geometry constant $Q = h/t$ plays a crucial role in determining the behavior of the bi-stable mechanism [26]. When the value of Q is in the range of 1.67–2.31, the curved beam will undergo instability buckling, resulting in negative stiffness behavior. When the Q value is greater than 2.31 and the second buckling mode is constrained, i.e., restraining z-axis torsion of the center of the curved beam, the curved beam will exhibit bi-stable behavior. One method to constrain the second mode is using a column to connect the two curved beams at their centers to form a double curved beam structure, as is shown in Fig. 2(b). In this structure, torsional deformation generated by the second mode of either curved beam converts to the axial deformation of another by the connecting column. Since the curved beam exhibits high rigidity in the axial direction, the second mode of either curved beam can be effectively constrained by another curved beam. In this work, the double curve beam with geometry constant $Q = 4$ is chosen as the bi-stable element.

2.2. Frame reinforced cell design

Curved beam honeycomb unit cell that uses curved beam is shown in Fig. 3(a), which is the most traditionally adopted form [35]. The unit cell comprises two sets of double curved beams and a supporting frame, where the supporting frame plays a crucial role in supporting the entire structure and providing boundary conditions for the double curved beams.

During the buckling process, the X-axial forces are inevitably generated at both ends of the curved beams. However, the stiffness provided by the supporting frame is limited, resulting in obvious bending deformation of the supporting frame. Therefore, the perfectly clamped-clamped condition that Qiu et al. used in the theoretical calculation is difficult to realize in this design method [26], leading to a large gap between actual and theoretical results. To further depict the influence of boundary condition provided by the supporting frame on

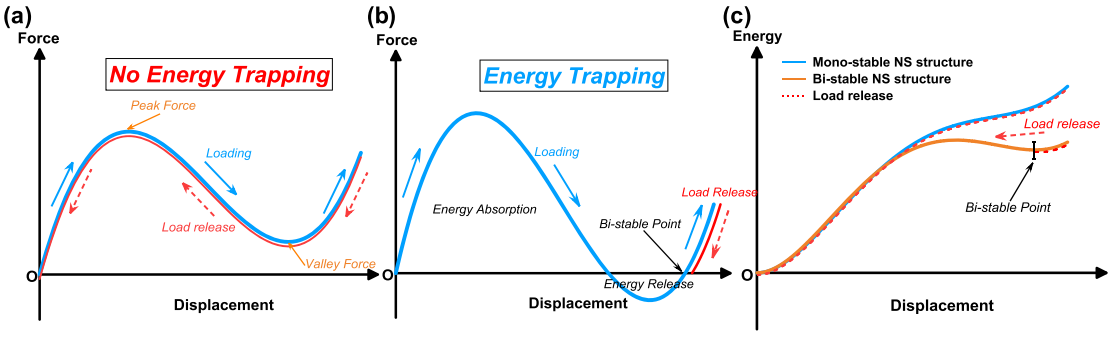

Fig. 1. Typical force-displacement relationship of (a) Mono-stable NS structure and (b) Bi-stable NS structure; (c) Energy-displacement relationship of mono-stable NS structure and bi-stable NS structure.

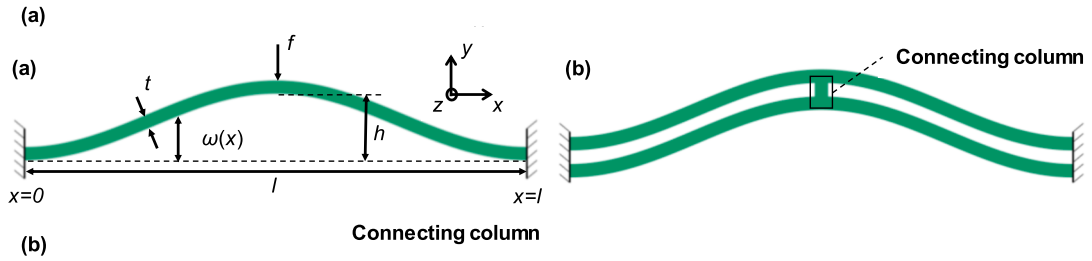

Fig. 2. The schematic of (a) the sinusoidal curved beam and (b) double curved beam design.

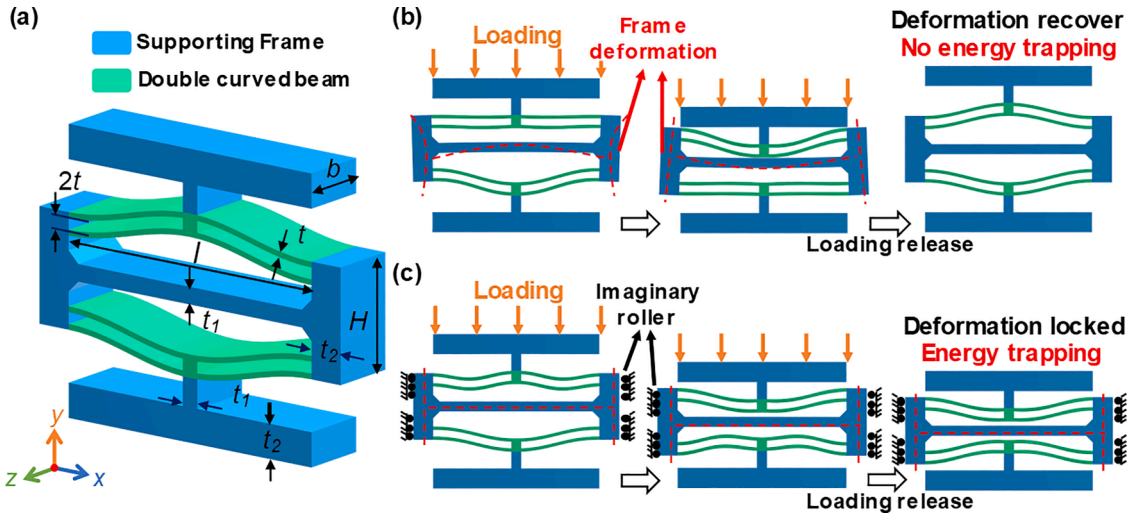

Fig. 3. Curved beam honeycomb unit cell: (a) Parameters schematic; Loading process and results for (b) the normal curved beam honeycomb unit cell and (c) the same curved beam honeycomb unit cell constrained by imaginary roller supports.

the structure, Fig. 3(b) and (c) illustrate the loading and loading release results obtained by the curved beam honeycomb unit cell and the same unit cell with imaginary roller supports on both sides, respectively. The imaginary roller supports act as a restrain to eliminate bending deformation in the frame, providing perfectly clamped-clamped condition. When the load is removed, the structure that relies solely on the supporting frame to constrain the deformation of the curved beam will restore its initial configuration. Conversely, the frame with imaginary roller supports will not return to its original configuration but instead maintain the compressed state, realizing energy trapping, which can be considered as efficient and effective configuration for energy absorption applications.

In this work, a novel FR unit cell is designed to minimize frame deformation without multiple unit cells in parallel. In this way, the mechanical performances of the fabricated sample will match that of the theoretical analysis. The design process of the supporting frame is depicted in Fig. 4. Firstly, the double curved beam is retained to constrain the second mode, while the axial forces from the two curved beams are distributed by increasing the height of the frame and the distance between the two beams. The metamaterial cells obtained by this method are named as spaced beam cells, as shown in Fig. 4(a). Subsequently, two reinforcing frames are introduced between the two sets of double curved beams correspondingly. A hole is incorporated in the middle of the reinforcing frames to allow the presence of the connecting column, as shown in Fig. 4(b). In the new design, the reinforcing frames provide additional stiffness and also reduce the arm of the X-axial force generated at both ends of the curved beams. Consequently, the bending deformation of the supporting frame reduces, providing an ideal clamped-clamped condition.

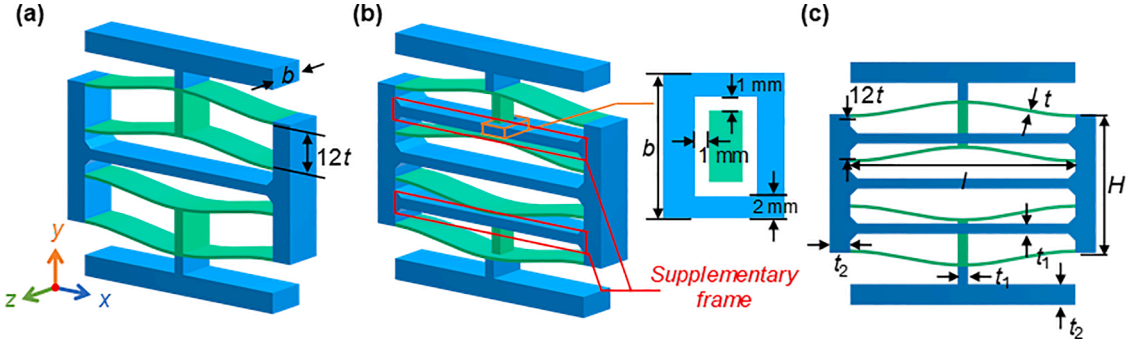

Fig. 4. The design process of the FR cell: (a) Spaced beams cell; (b) The proposed FR unit cell; (c) Parameters schematic of the novel FR cell.

3. Numerical simulation

In this section, numerical simulation is conducted to measure the mechanical properties of three types of unit cells with identical parameters. Moreover, a pair of metrics is proposed to evaluate the bi-stable behavior of unit cells quantitatively, and to demonstrate the superior bi-stable behavior compared with the curved beam honeycomb cell. Finally, the optimal parameters selection method, which considers the properties of the base material, is outputted by parametric analysis. All initial models are modelled by SolidWorks software, and the finite element (FE) software ABAQUS was used to carry out the numerical simulations. Finite element analysis was based on the implicit analysis, which is suitable for quasi-static analyses. Geometrical nonlinearity was considered in the finite element models to account for the snap-through behavior of the structure. The tetrahedron element C3D10 was used to mesh the model, and mesh convergence tests were conducted to ensure accuracy. The FE analysis utilized a linear elastic material model, with Polyamide (PA) selected as the base material ($E = 1300$ MPa, $\rho = 1100$ kg/m^3, and $\nu = 0.34$). The front views of all FE models are shown in Fig. 5. A downward displacement-controlled load of 4 mm/min is applied at the reference point (RP) on the upper load plate of the model, while the bottom plate of the model was fixed. The reaction force and displacement were monitored to obtain the force-displacement curve of the structure under compression.

3.1. Static behavior

The FE models were employed to compare the mechanical response of the curved beam honeycomb unit cell, spaced unit cell, and the novel FR unit cell. Furthermore, structures consisting of two to six of the above three different unit cells in parallel are also simulated to examine their energy absorption capacity and bi-stable performance. The parameters of the FE model are provided in Table 1, with the curved beam in all three unit cells sharing identical parameters. Except for the frame height H, all other parameters of the frame remain identical across the different unit cells.

The mechanical properties of the three types of unit cells under compressive load were analyzed through numerical simulations, and the corresponding force-displacement curves are presented in Fig. 6(a). Firstly, the curved beam honeycomb unit cell exhibits a peak force of 12.9N and a valley force of 6.1N. The valley force is greater than zero, indicating that the curved beam honeycomb element cannot achieve bi-stable state, even if its curved beam parameters meet the requirements of theoretical calculation. Notably, the peak force caused by the second buckling is lower than the first peak force, and the displacement from the second buckling to the recovery of positive stiffness is also shorter. The reason behind this phenomenon is that the frame deformation caused by first buckling reduces the constraining force of the support frame. The spaced cell also shows a mono-stable performance, although a reduction in the valley force to 3.5N and an increase in the peak force to 13.2N are observed. Subsequently, the novel FR cell demonstrates significantly superior performance. The peak force value is seen as 19.4N, which increases by approximately 50 % compared to the curved beam honeycomb cell, indicating its enhanced energy absorption capability. The valley force is -3.2N, indicating that the novel FR cell possesses sufficient strength and provides stronger constraints for curved beams, resulting in expected bi-stable behavior and energy trapping. In addition, the force-displacement curve of the ideal cell with imaginary roller support is given in the picture, with peak and trough forces of 21.9N and -6.1N, respectively. The comparison indicates that the mechanical response of the FR unit closely matches that of the ideal unit, in terms of the shape of the curve and the value of peak force and valley force.

Table 1
Parameters of FE models (unit: mm).

Parameter	Curved beam				Frame		
	h	t	l	b	t_1	t_2	H
Honeycomb cell	4	1	65	12	3	6	20
Spaced cell	4	1	65	12	3	6	40
FR cell	4	1	65	12	3	6	40

The results for two unit cells arranged in parallel are shown in Fig. 6 (b). When comparing three types of cells, the findings are consistent with those of a single cell. Specifically, the honeycomb cell structure has peak and valley forces of 32.5N and 2.9N, respectively. The spaced cell structure shows peak and valley forces of 32.7N and 2N, respectively. It is clear that the forces of the structures with honeycomb cells and spaced cells in parallel do not double up the force of a single unit as expected. This enhancement in performance is attributed to the middle supporting frame of the parallel units, which is subjected to opposing forces from

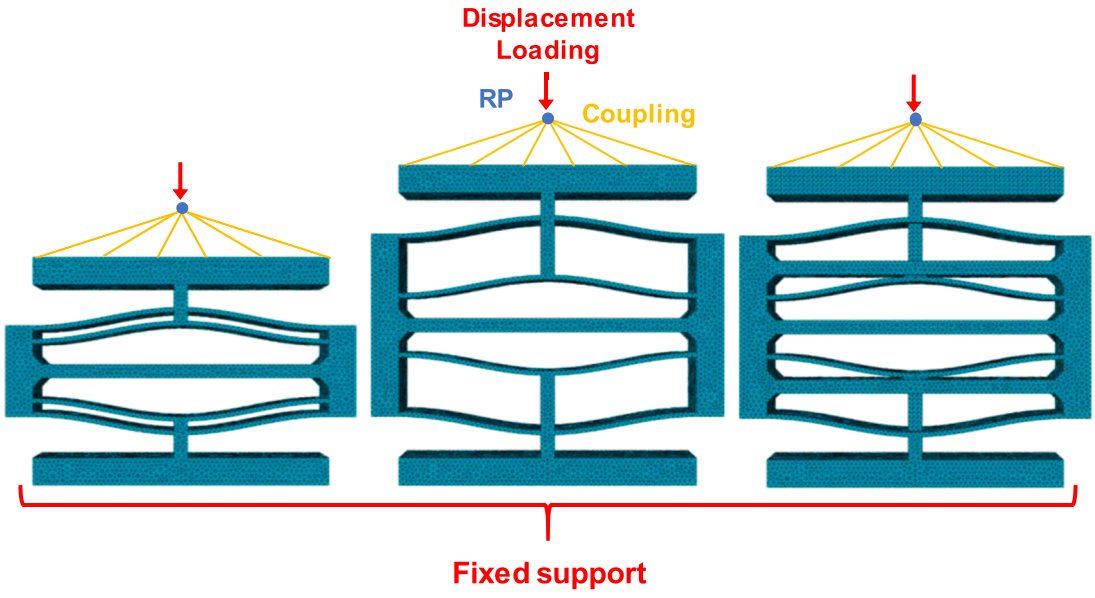

Fig. 5. The FE model of three types of unit cells.

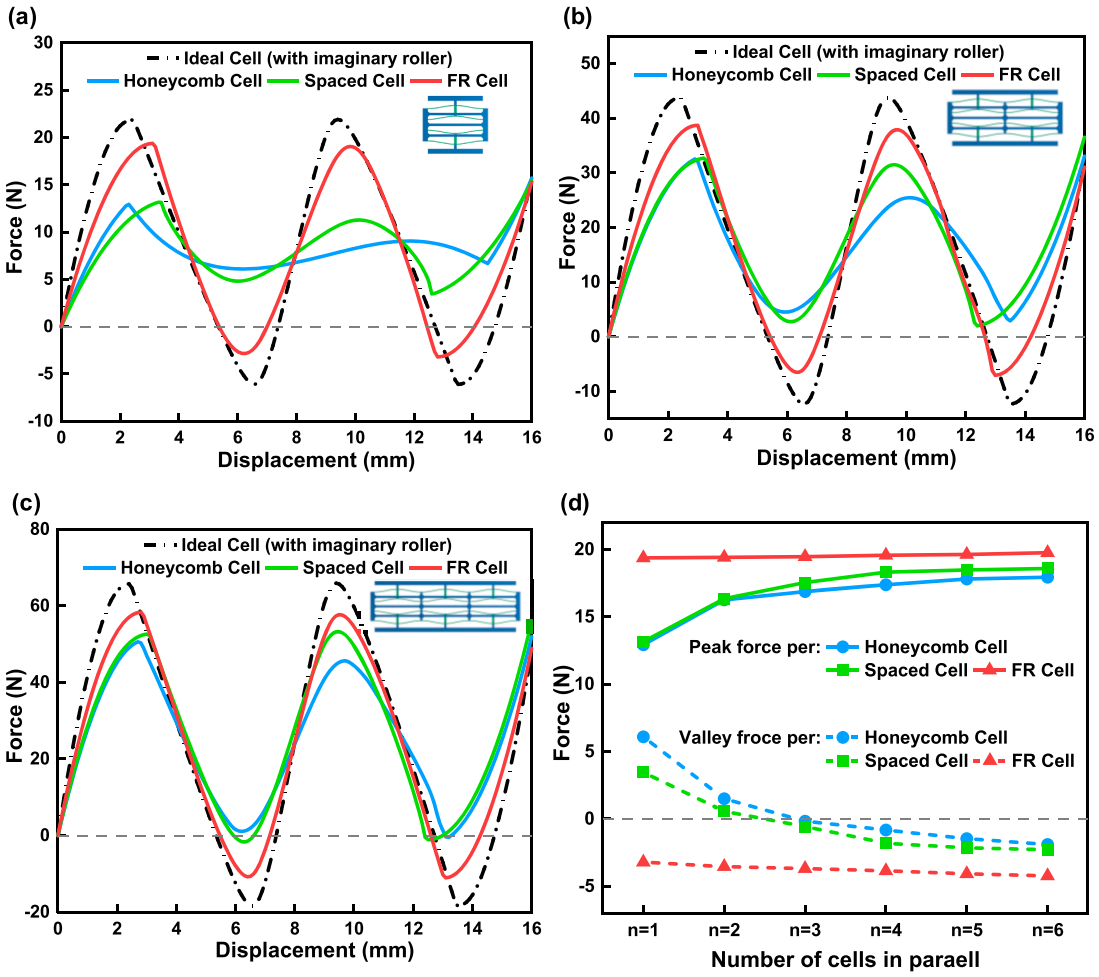

Fig. 6. The static mechanical response of novel FR cell, honeycomb cell and spaced cell obtained by simulation: (a) Single cell; (b) Two cells in parallel; (c) Three cells in parallel; (d) The change of the peak force and valley force provided by each cell.

the curved beams on each side and thus cancel off. As a result, the deformation of the supporting frame is reduced, providing stronger constraints to the curved beams and resulting in increased peak force and decreased valley force. However, despite the improvement in mechanical properties, the overall structure remains mono-stable when two honeycomb cells or spaced cells are placed in parallel. Moreover, the discrepancy in the support strength of each side of the beam may result in uneven deformation of the curved beam. In contrast, the FR cell structure exhibits a peak force of 38.7N and a valley force of -7N, which are almost twice as much as a single FR cell, indicating that the mechanical properties of FR cells in parallel are to be predicted.

In the case of three cells placed in parallel, the simulation results are shown in Fig. 6(c). The peak force of the FR structure changes to 58.4N, which is accurately three folds of a single FR cell. The curved beam honeycomb structure and spaced structure exhibit a valley force of -0.5N and -1.67N, indicating that both structures exhibit bi-stable behavior. However, their peak forces reach 50.3N and 53.28N, which is more than four times the peak force of a single cell. It is obvious that the peak force and valley force changes are not linear, and this may introduce uncertainty into structure design and properties predicting if a programmable metamaterial is to be designed.

To evaluate the contribution of a cell unit to the overall structure, the average peak and valley forces per cell, with varying numbers of cells arranged in parallel, are illustrated in Fig. 6(d). This value is obtained by dividing the peak or valley force by the number of cells in the structure. Taking the solid red line as an example, the six values on the line represent the peak force provided by each FR cell in the structure consisting of 1–6 FR cells. As expected, as the number of cells in parallel increases, the average peak forces provided by each curved beam honeycomb cell or spaced cell increase while the valley force decreases, with a diminishing magnitude of change. In the case of the FR cell, the peak force and valley force provided by each cell remain nearly unchanged regardless of the number of cells. This provides a great foundation for building a programmable metamaterial, e.g., the mechanical response of a structure composed of novel FR cells is relatively predictable. However, for the other two types of cells, the linear trend is only exhibited when the number of parallel connections is higher than six, inevitably leading to inefficient use of space and material. As a result, when designing metamaterials, the use of FR cell allows researchers to select the number of metamaterials cells according to actual requirements and reduces the amount of work involved in the design and validation process.

3.2. Bi-stable behavior

Analyzing and evaluating the bi-stable behavior of different bi-stable structures can be challenging because various factors can produce an effect on the bi-stable behavior of the structure. In the force-displacement curve, the peak force represents the buckling threshold of the structure and relates to the bearing capacity of the structure. On the other hand, the valley force plays a crucial role in achieving bi-stable behavior. A smaller valley force indicates a more stable bi-stable state for the structure, meaning that the structure can maintain its compressed stable state against greater disturbance. However, it is essential

to note that a smaller valley force also implies a higher amount of energy can be released during the transition from the original stable state to the compressed stable state. As a result, the overall energy absorption capacity of the structure may be lower. Therefore, evaluating the bi-stable behavior requires considering both the peak and valley forces.

This work proposes a new metric φ to quantitatively evaluate the bi-stable properties, as shown in Eq. (2).

$$\varphi = \left[\frac{F_P}{F_{Pr} - F_{Vr}}, \frac{F_V}{F_{Pr} - F_{Vr}}\right] \tag{2}$$

where F_P and F_v represent the peak force and valley force of the structure, respectively; F_{Pr} and F_{Vr} represent the peak force and valley force of the same structure with imaginary roller support. For the structure with given parameters, the bi-stable performance of the structure with roller support is optimal. Therefore, φ obtained from the structure with roller support can be used as a reference to evaluate the bi-stable behavior of different structures.

The evaluation of bi-stable behaviors of three kinds of cells using the proposed metric is shown in Fig. 7. The upper and lower boundaries of the bar chart represent the first and second values of φ, respectively. The dotted lines at the top and bottom represent the ratio of F_{Pr} and F_{Vr} to F_{Pr} - F_{Vr}. If the lower section of the bar chart is above 0, it means that the structure does not possess bi-stable ability. It can be observed that the bi-stable performance of the FR structure maintains around 80 % of the reference value as the number of cells in parallel increases. On the other hand, the honeycomb structure and spaced structure show an increase from 40 % and 50 % to 73 % and 75 %, respectively, as the number of parallel cells increases from 1 to 6. Moreover, the bi-stable properties φ of both honeycomb cell and spaced cell hardly change when the number of parallel cells increases from 5 to 6, indicating that the bi-stable properties of structures will not be enhanced even if more unit cells are arranged in parallel when the number is larger than 6, but it is clear that the bi-stable properties are still inferior to FR cells.

Obviously, the proposed FR cell has more constant bi-stable properties compared to other cells, which provides convenience for designing programmable multi-stable metamaterials. The FR multi-stable metamaterials can be fabricated as a whole structure directly by additive manufacturing technology, and the multi-stable properties have a predictable linear relationship with the number of unit cells. This provides an easier and faster method for customizing and designing metamaterial according to requirements, as well as for the manufacture of metamaterial.

3.3. Parametric analysis for FR cell

Parametric analysis is conducted to provide guidance for selecting the raw material of metamaterial and the optimal curved beam parameters. The parametric analysis focuses on the curved beam thickness t and height h, which are parameters related to the geometric constant Q. The force-displacement responses of the structures with parameter t varied from 0.5 mm to 2.5 mm with step of 0.1 mm, while h varied from 2.5 mm to 5 mm with step of 0.1 mm, are obtained through simulations. The other parameters, length l and depth b, are 65 mm and 12 mm, respectively. Furthermore, the parametric analysis model sets the frame height H as a function of the curved beam height h to avoid contact of the center of the curved beam with the frame when it reaches the maximum displacement.

Fig. 8(a) and (b) illustrate the bi-stable and negative stiffness area of the honeycomb cell and FR cell obtained by parametric analysis of t and h. The bi-stable or negative stiffness area refers to the region consisting of all parameter combinations that enable the unit cell to exhibit bi-stable or negative stiffness behavior. Notably, in this figure, the ratio of the valley force to the peak force, α, is used to classify the properties that the unit cell exhibits for the combination of different t and h. The value equal $\alpha = 1$ means that the force-displacement curve of the structure under this parameter is monotonic and has no extreme points, indicating that the structure is mono-stable and does not exhibit negative stiffness. An α value between 0 and 1 signifies that the valley force is greater than 0, and the structure is still mono-stable but exhibits negative stiffness behavior. A value less than 0 indicates that the valley force is lower than 0, and the structure under this parameter is bi-stable. As shown in Fig. 8, the bi-stable area of the novel FR cell expands by approximately 67.1 % compared to the honeycomb cell within the considered parameter range. The negative stiffness area also increases by 46.3 %. Besides, whether designing multi-stable or negative stiffness metamaterial, FR cells have a wider choice of parameters than honeycomb cells, providing more design options.

Fig. 9 analyses the specific energy trapping (SET) and the maximum strain value generated during the deformation of the FR cell for different parameters, which can provide guidance for the original design of the metamaterial as well as the selection of base material. The specific energy trapping, denoted as W_m, represents the energy trapping per unit mass and can be expressed as follows:

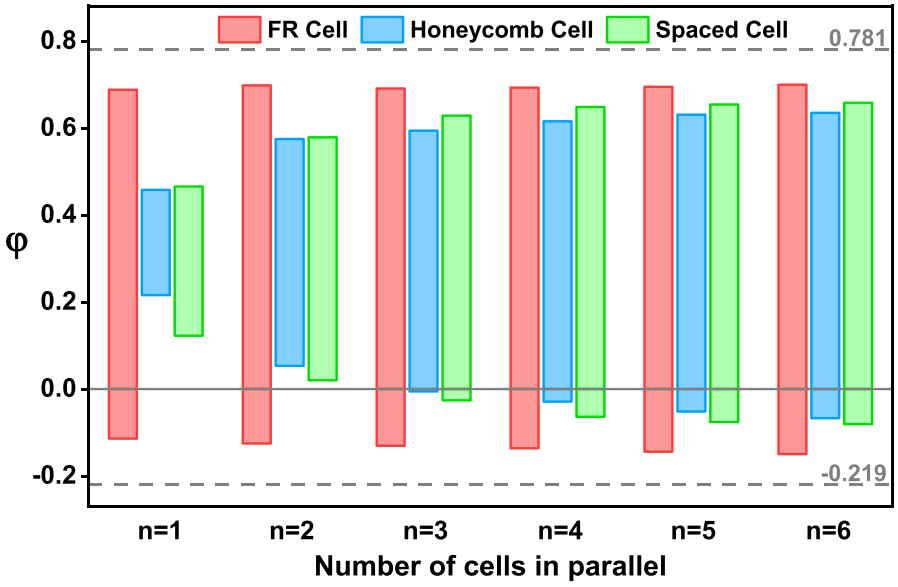

Fig. 7. The bi-stable properties of three types of cells.

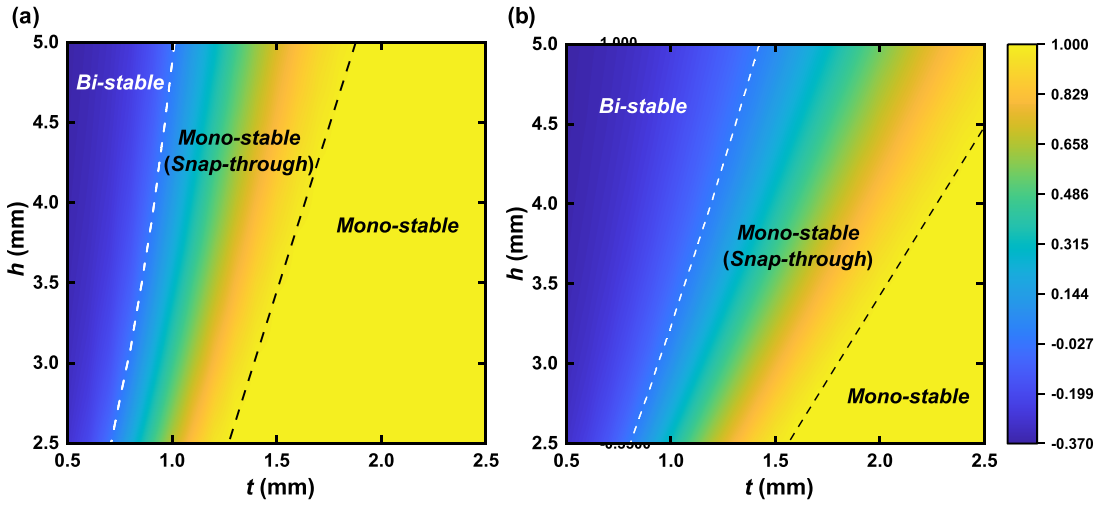

Fig. 8. Parametric analysis of properties classification indicator α: (a) Honeycomb cell; (b) FR cell.

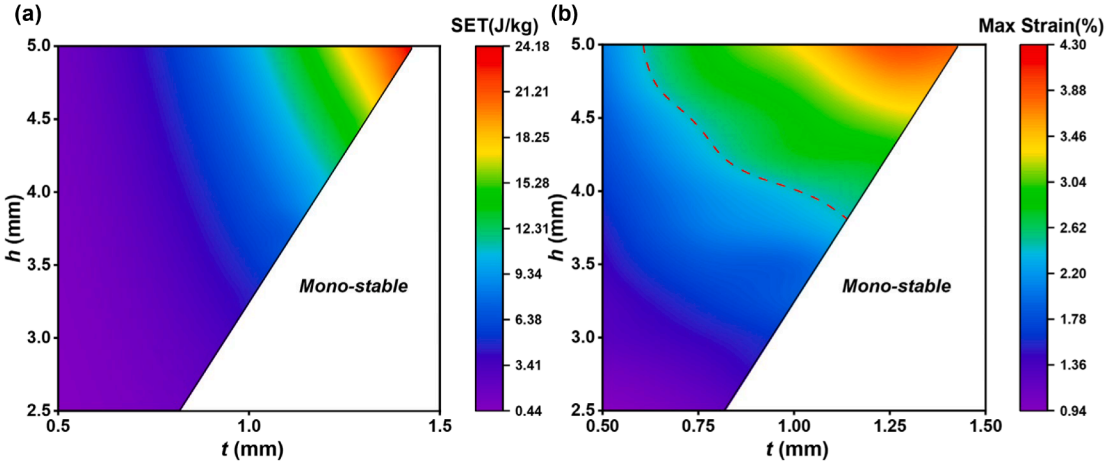

Fig. 9. Effect of t and h on (a) SET and (b) maximum strain during the deformation process.

$$W_m = \frac{W_T}{V\rho} \tag{3}$$

$$W_T = \int_0^{D_b} F(\delta)d\delta \tag{4}$$

where W_T means the trapped energy by the structure; ρ is the density of base material; D_b is the deformation corresponding to the bi-stable point. The volume of the whole structure, V, can be obtained by adding up the volume of the supporting frame and the curved beam.

The relationship between specific energy trapping (SET), maximum strain, and the parameters t and h is analyzed and depicted in Fig. 9. As depicted in Fig. 9(a), the specific energy trapping improves with increasing values of t and h. Moreover, as the value of h increases, the energy trapping per unit mass, Wm, becomes more sensitive to the variations in t. A similar trend can be observed in Fig. 9(b), indicating that the maximum strain during compression increases with increasing values of t and h, which means that the maximum strain of the structure increases as it acquires more extraordinary energy trapping ability. Based on the consideration of the mechanical properties and reusability, it is crucial to consider both the specific energy trapping and the maximum strain, as well as the elastic limits of the material. In the next section, we select Polyamide 12 as the base material for experimental specimen fabrication. According to the elastic limit of Polyamide 12, the maximum parameters that can be selected are shown as the red dotted line in Fig. 9(b). Finally, considering both the specific energy trapping and the requirement of manufacturing accuracy, t and h are chosen to be 1 mm and 4 mm, respectively.

4. Experiment

To verify the mechanical performance and programmability of the designed novel FR cell, quasi-static tests and impact tests were conducted. Results obtained by quasi-static tests of 1×1 cells are used to predict the mechanical response of 2×2 metamaterial, and the comparison between prediction and actual test results is applied to prove the programmable properties of the proposed metamaterial. The complexity of the novel FR structure, particularly the connection between the two curved beams that need to pass through a frame beam, presents challenges for traditional manufacturing techniques. However, the use of advanced manufacturing technology, specifically additive manufacturing (3D printing), offers a viable solution. In this section, all samples were fabricated using the additive manufacturing method called Multi Jet Fusion (MJF) with Polyamide 12 (PA12) material.

4.1. Quasi-static tests of 1×1 cell

Quasi-static compression tests are performed to investigate the mechanical behavior of the structure. The MTS Electromechanical Uni-

versal Testing Machine E42.503, with 5 kN force capacity and 5.1×10^{-5} mm resolution, is used to conduct compressive tests along the vertical direction. The experiment is conducted under displacement control with a constant loading rate of 4 mm/min to minimize dynamic effect. The bottom edge of the specimen fully fixed to the loading plates by glue (Loctite 401) to the test machine. During compression, the reaction force of the specimen is collected by the force sensor of the testing machine with sampling frequency of 100 Hz. Furthermore, the results of the compression tests are used to validate the numerical model.

Two types of structures, namely the 1×1 and 2×2 metamaterial structures, are tested to evaluate their mechanical properties under quasi-static conditions. The 1×1 structure consists of a single novel FR cell, while the 2×2 structure comprises four cells, as depicted in Fig. 10 (a). The unit cell used in the experiments has the same parameters as the FR cell described in Table 1. The material properties of the used PA 12 raw material are characterized by standard tensile measurements according to ASTM D638–14, as illustrated in Fig. 10(b). The date of material properties is used in finite element analysis to compare with the test results.

The force-displacement curve for the 1×1 structure, along with the energy-displacement curve and corresponding picture of compression test processes, are presented in Fig. 11(a)–(c). The force-displacement curve exhibits two regions of negative stiffness, corresponding to two layers of double curved beam. Besides, peak forces are 19.17N and 20.57N, and valley forces are -3.4N and -3.35N, respectively, which agree with the finite element model quite well. The experimental force-displacement response aligns well with the simulation, further confirming the accuracy of the proposed finite element (FE) model. Moreover, the deformation patterns observed in the structure at various compression stages closely match the results obtained from the FE model. The recorded valley force is negative, indicating that the metamaterial cell retains the compressed configuration after unloading.

Notably, the 1×1 structure consists of two layers of bi-stable elements, and the snap-through behavior of the curved beam occurs layer by layer rather than buckling simultaneously. Thus, the 1×1 structure has three stable positions, i.e., the origin stable position, the first stable position, and the second stable position, as shown in Fig. 11(b). The three stable positions divide the compression process of the structure into two stages, each corresponding to a process during which the structure absorbs energy and releases some of it so that the stable positions represent the local minimum point of the energy. Meanwhile, the energy corresponding to the second stable position and third stable position represents that the structure trapped energy of 55.67 mJ and 119.77 mJ after undergoing one layer and two layers of curved beam compressed.

The programmable property of the proposed metamaterial allows the mechanical properties of multi-unit metamaterials to be predicted by the mechanical properties of the unit as well as the number of units, which can be used to verify programmability. According to the force-displacement curve of the 1×1 cell obtained by compression test, it can be inferred that the peak force and valley force of 2×2 metamaterial are about 39.2N and -6.7N, respectively. Moreover, the appearance of four negative stiffness stages can also be predicted, indicating that the structure has four energy trapping points, and the corresponding energy values can be concluded to be 120 mJ, 240 mJ, 360 mJ and 480 mJ according to the programmable properties.

4.2. Quasi-static tests of 2×2 metamaterial

Quasi-static tests of 2×2 metamaterial are conducted to verify the accuracy of the prediction. Fig. 12(a) displays the force-displacement curves obtained from the experiment and simulation of the 2×2 metamaterial structure. The test results and the predictions show good agreement, and four spaced negative stiffness stages are observed in both the test and simulation results. Besides, the peak force and valley force predicted by programmability are also verified with average values of 40N and -6.1N, respectively. Furthermore, due to manufacturing errors associated with the MJF technology, the four layers of curved beams in the 2×2 sample are not identical, resulting in varying buckling forces for each layer [19]. During the compression test, the weaker layer tends to buckle earlier than the stronger layer. As a result, the force-displacement curve obtained from the experiment demonstrates an increasing trend with each successive peak force. The influence of this inevitable phenomenon is most apparent in the last peak force, which is nearly 1N higher than the first three peak forces.

Fig. 12(b) and (c) present the energy-displacement curve and five stable positions of the 2×2 metamaterial structure in the compression test and simulation, with the red box indicating the curved beam of this layer in the compacting stage. Similar to the 1×1 structure, the snap-through behavior of each layer occurs separately, so four layers of bi-stable curved beams correspond to five stable positions as well as energy trapping points. The energies corresponding to the last four stable positions represent the energies that the 2×2 structure can trap at different stages, which are 143 mJ,287 mJ,422 mJ and 556 mJ, respectively. Since the energy accumulates and each peak force is approximately 1N higher than the predicted value, the difference in energy at each energy trapping point compared to the predicted value is greater than at the previous point. However, the energy levels corresponding to each energy trapping point remain within an acceptable range of the predicted values in practical applications, demonstrated by that the discrepancy accumulated by each stable position is less than 4 %.

The programmability of the metamaterial is successfully verified by the method of experiments and prediction. The whole metamaterial can be fabricated at one time by additive manufacturing without requiring other steps, simplifying the process of actual production. In addition,

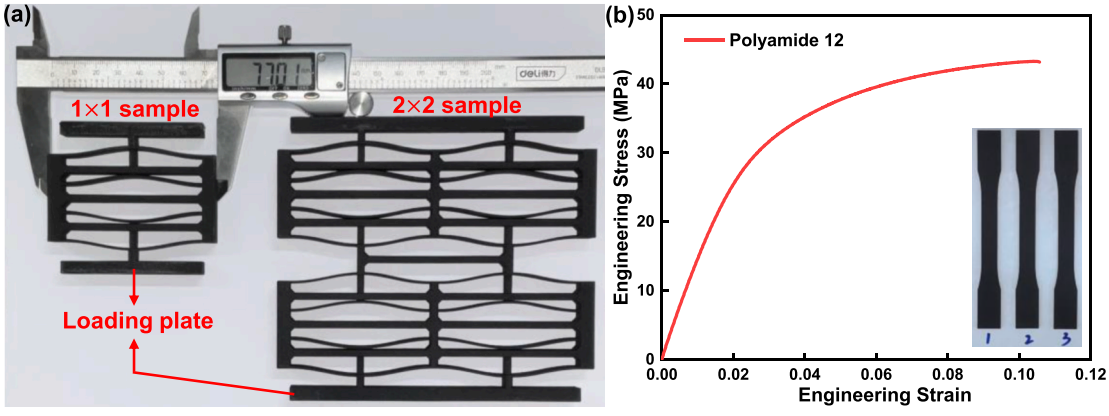

Fig. 10. Test samples and raw material properties: (a) 1×1 and 2×2 multi-stable metamaterial sample; (b) Stress-Strain curve of Polyamide 12.

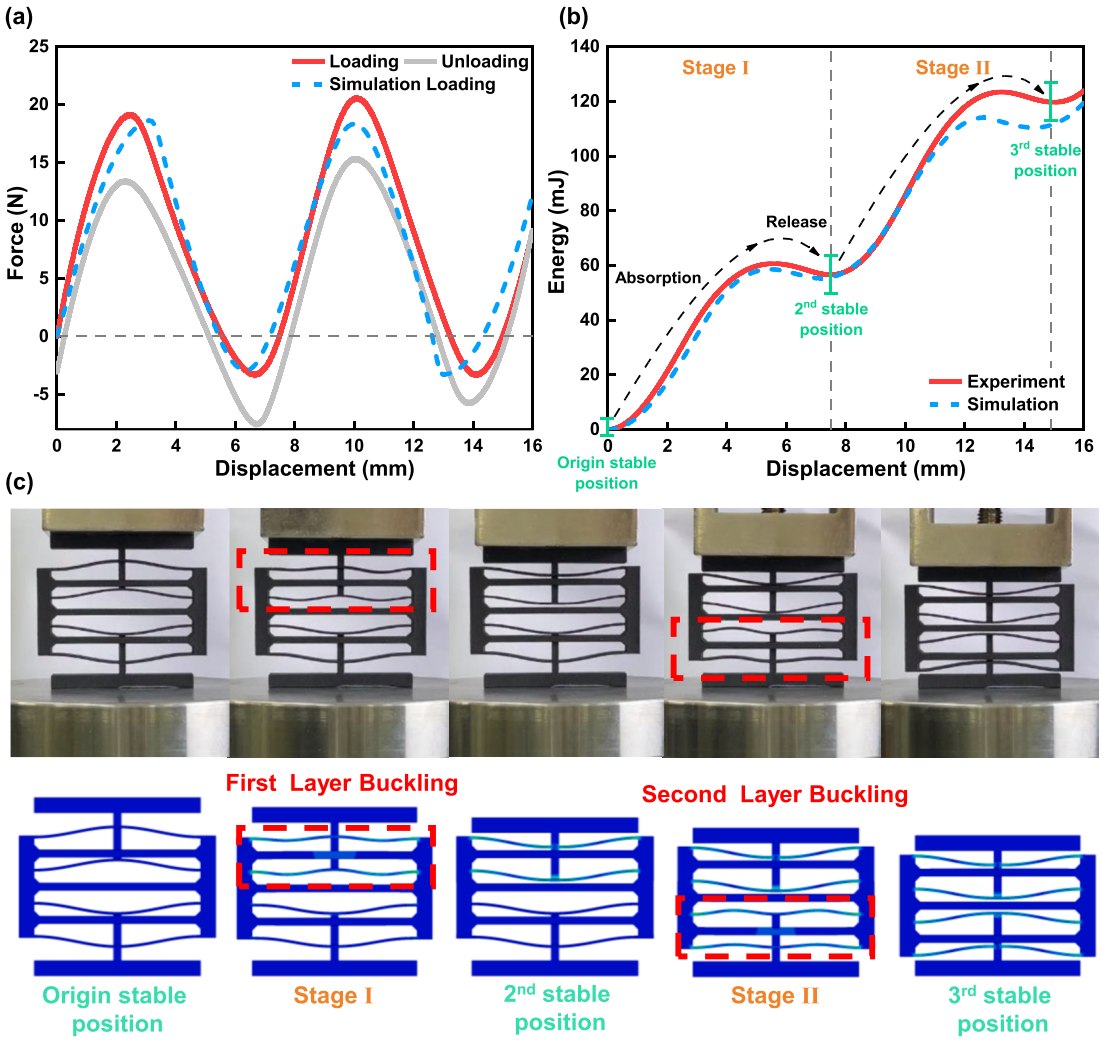

Fig. 11. The results of 1 × 1 structure obtained by quasi-static test and simulation: (a) Force-displacement response; (b) Energy-displacement curve; (c) Deformation process.

unlike previous studies, the programmable properties of the metamaterial can be realized on the basis that all cells are connected closely in parallel and series, reducing the space utilization of the metamaterial.

4.3. Impact testing

Plate-impact tests were conducted to investigate the cushion performance of the multi-stable structure composed of novel FR cells. The impact test apparatus and its schematic diagram are shown in Fig. 13(a), (b) and (c), respectively. The system primarily comprises the following components: an impact plate and slides, which together constitute an impact mass of approximately 400 g, two low-friction linear guideways that guide the impact plate to excite the samples, a dynamic data acquisition device, an acceleration sensor and a force sensor to record the acceleration and force responses during the impact process, and a heavy metal plate fixed at the bottom of the frames, serving as the reaction mass for the frame and the specimen holder.

The impact tests were conducted with the impactor released from different heights, and the acceleration responses were recorded to assess the cushioning property of the designed multi-stable structure. The test results were analyzed and explained through structural threshold force and energy trapping mechanism Besides, a comparative investigation on the acceleration response of the uncompressed multi-stable metamaterial and the compressed metamaterial was carried out to analyze the influence of multi-stable behavior on the cushion property of the structure. The compressed structure represents that the same structure is compressed to the fifth stable position so that it cannot trap energy through multi-stable transforming when upon impact.

Fig. 14(a) shows the complete response history of the impact with the uncompressed 2 × 2 multi-stable metamaterial from heights of 0.2 m to 0.35 m. Here, the whole acceleration-time curve can be divided into three stages, namely stage I (the free-fall stage), stage II (the impact stage) and stage III (the rebound stage). Stage I refers to when the impactor is still in free falling and has not contacted the 2 × 2 multi-stable structure. In stage II, the impactor charged the 2 × 2 multi-stable structure, and the curved beams undergo elastic instability and trap the energy through the bi-stable mechanism. In the last stage, the small amount of energy not trapped by the structure results in several small rebounds of the impactor, eventually returning the acceleration to 0 as the energy is dissipated. In addition, the force-time curve shown in Fig. 14(d) exhibits three stages. In the first stage, the force value remains at 0N, indicating no impact at the time. In the second stage, the specimen is impacted by the plate, and force peaks appear on the curve. In the third stage, after undergoing several rebounds, the impact plate presses stably on the specimen, and the curve ultimately stabilizes at 4N. This final force value corresponds to the mass of the impact plate, which is 400 g.

Besides, an acceleration threshold appears and remains almost constant regardless of the impact heights. The magnitude of this threshold correlates with the peak force of the multi-stable structure and can be

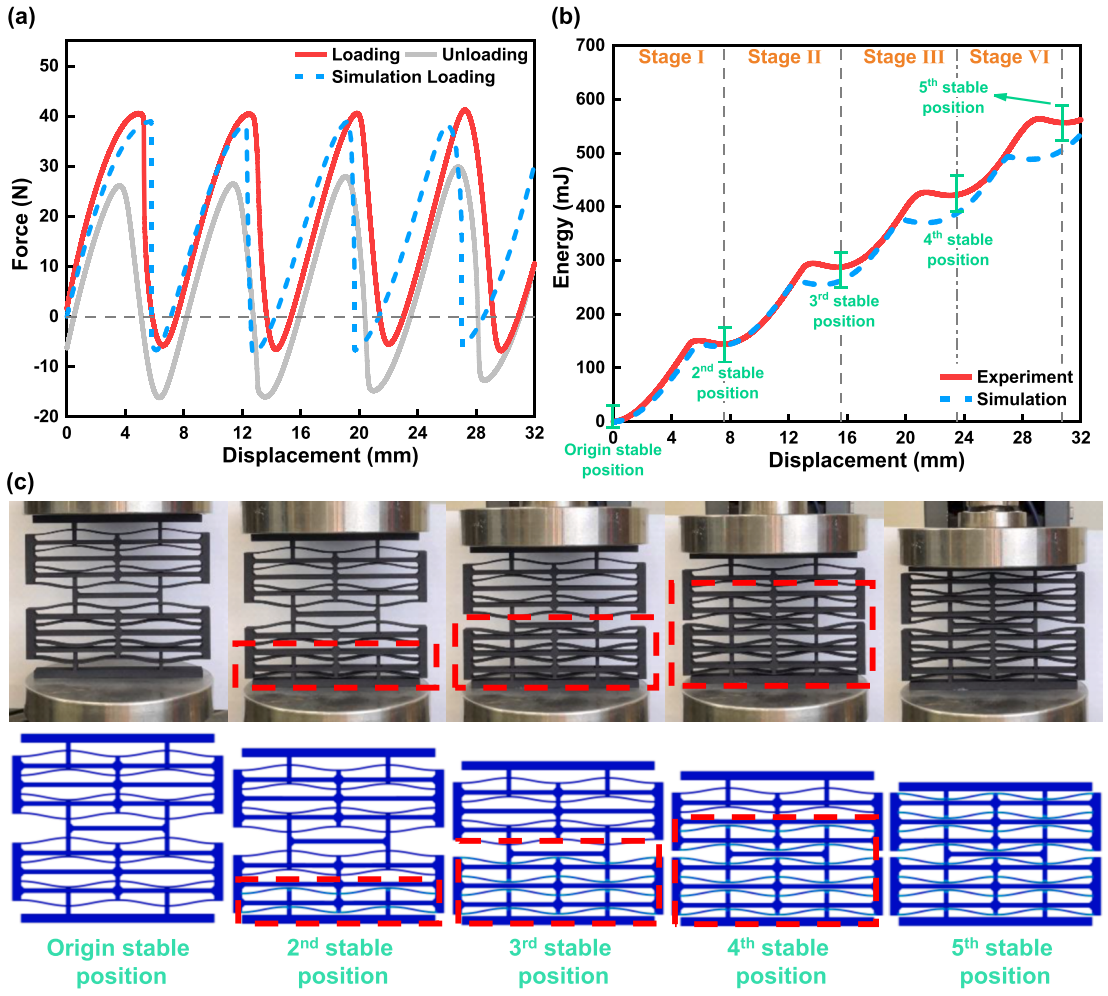

Fig. 12. The results of 2 × 2 structure obtained by quasi-static test and finite element simulation: (a) Force-displacement response; (b) Energy-displacement curve; (c) Deformation process.

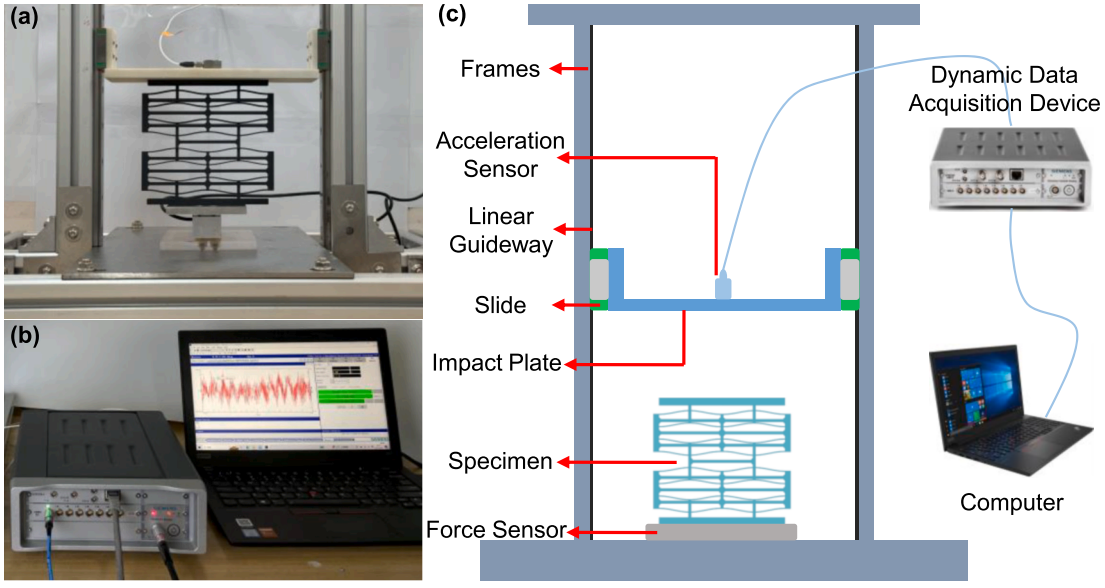

Fig. 13. Plate impact test: (a)Test apparatus; (b) Dynamic Data Acquisition System; (c) Schematic diagram of impact test apparatus.

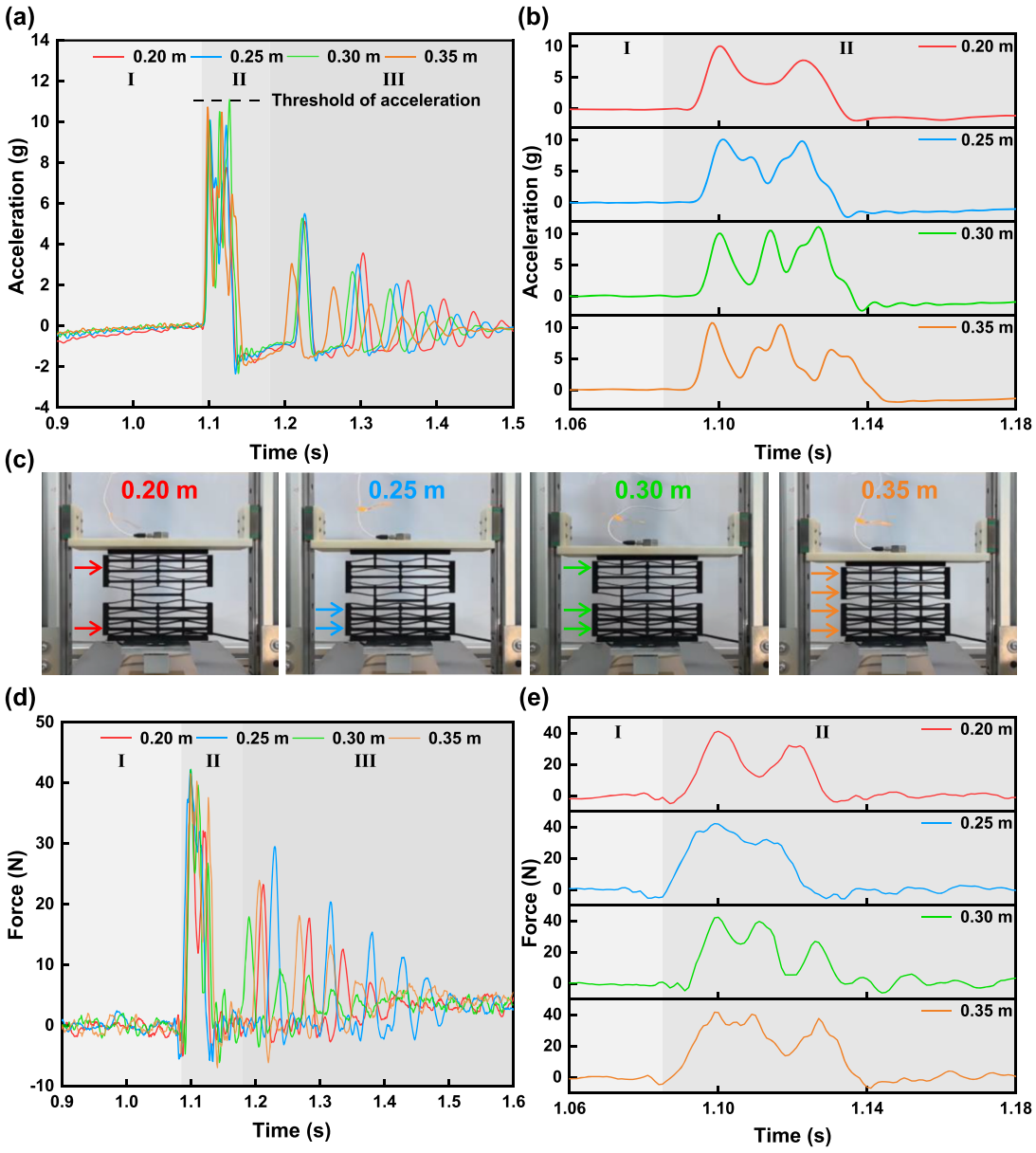

Fig. 14. Results of plate impact testing: (a) The complete acceleration response history of the impactor falling from heights of 0.2 m, 0.25 m, 0.3 m and 0.35 m for 2 × 2 multi-stable metamaterial; (b) The acceleration response of the 2 × 2 multi-stable metamaterial in stage II; (c) Snapshots of specimens after the impact test (d) The complete force response history of the impactor falling from heights of 0.2 m, 0.25 m, 0.3 m and 0.35 m for 2 × 2 multi-stable metamaterial (e) The force response of the 2 × 2 multi-stable metamaterial in stage II.

calculated using the following equation [22,36]: $a_{th} = F_P / m = 40N / 0.4kg = 100 = 10g$, where a_{th} is the acceleration response threshold, m is the weight of the impactor, and F_P is the peak force value of the corresponding structure obtained in the static compression tests. The impact forces of the second stage are shown in detail in Fig. 14(e), which effectively validates the accuracy of the equation.

The detailed acceleration and force responses at different impact heights during stage II are presented in Fig. 14(b). Each impact generates multiple acceleration peaks in stage II, and the amplitudes of these peaks are nearly uniform across different heights, corresponding to the threshold depicted in Fig. 14(a). Fig. 14(c) illustrates the specimens after the impact test of different heights, and the arrows indicate the location and number of compressed curved beam layers of the metamaterial after impact. At an impact height of 0.35 m, the metamaterial was completely compressed and produced four acceleration peaks. However, except for the case of complete compression, the test results do not exhibit a consistent relationship between the number of acceleration peaks and the number of compressed layers [37]. This is related to the fact that the energy trapping behavior of multi-stable metamaterials does not occur continuously. For multi-stable structures, the bi-stable mechanism is triggered only when the input energy exceeds a certain threshold, as indicated by the local maximum points in Figs. 11(b) and 12(b). This means that impacts with energies above a certain threshold and less than the next threshold will produce the same result, compressing the same number of layers of curved beams. However, an impact with energy close to the next threshold will obviously produce one more acceleration peak than an impact with energy close to this threshold.

Fig. 15(a) shows the acceleration history of an impactor released from a height of 0.3 m, colliding with both uncompressed and compressed structures. The results indicate that the multi-stable behavior of the uncompressed structure reduces the peak acceleration response by approximately 80 % and decreases the impact response time by 50 %. Fig. 15(b) shows the acceleration responses obtained from three impact tests on the same multi-stable structure at the same height. The

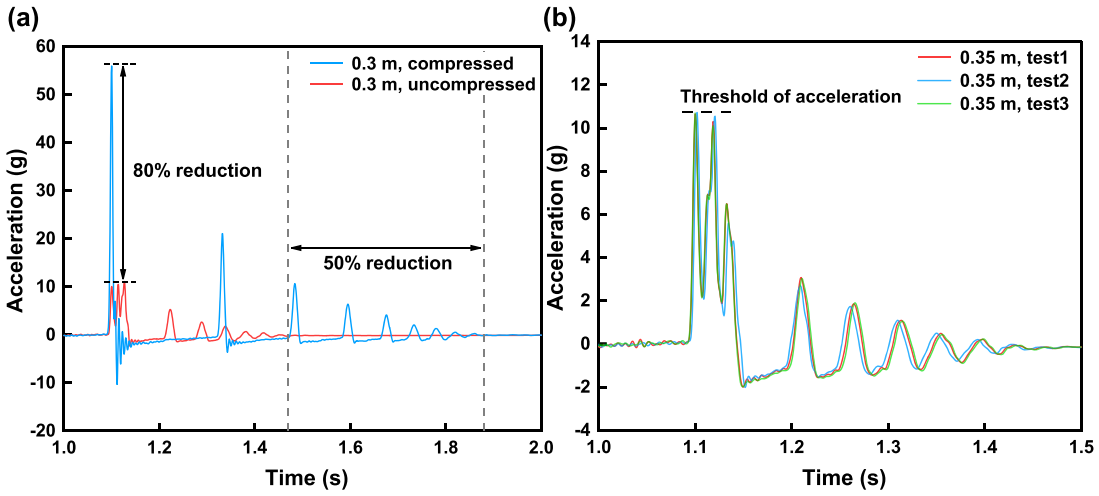

Fig. 15. Results of cushion performance and repeatable performance tests: (a) The acceleration responses of the uncompressed and compressed multi-stable metamaterial with impact height of 0.3 m (b) Repeated test on the 2×2 multi-stable metamaterial with impact height of 0.35 m.

acceleration responses from the three tests match very well which suggests that the proposed multi-stable metamaterial structure is highly repeatable.

In addition, since the energy trapping behavior does not occur continuously, and a small amount of residual energy accounts for the slight rebound observed in the third stage. Thus, minimal rebound occurs when the kinetic energy of the impactor is precisely sufficient to convert the multi-stable metamaterial to any stable position except the original one. The proposed FR cell enables the programming of the bi-stable properties of multi-stable metamaterial, including the triggering energy of the bi-stable mechanism. In practical applications, setting the triggering energy of multi-stable metamaterial reasonably according to the possible impact size of the different scenes is a suitable choice, which can minimize the impact rebound and reduce the damage of the impact.

5. Conclusion

This work proposes a novel FR cell developed to improve the bi-stable behavior and energy trapping efficiency of traditional curved beam cells, offering potential to design programmable metamaterials. The mechanical properties of three cell types with the same curved beam specifications are comparatively analyzed. Parametric analysis is conducted to study the influence of curved beam parameters on bi-stable behavior and energy trapping performance. Finally, static tests on 1×1 unit cell and 2×2 metamaterial samples are conducted to validate the results of finite element analysis of the programmable feature of the proposed FR cell. The plate-impact test is conducted to study the cushion performance of the multi-stable metamaterial. It is concluded that the novel FR configuration demonstrates superior mechanical properties, both in single-cell and multi-cell parallel arrangements, with predictable linear relationships. The FR design allows the curved beam to achieve bi-stable state over a wider range of parameters and enables it to obtain mechanical properties closer to the results predicted by theory, which increases the flexibility of designing multi-stable metamaterials. The fabricated novel multi-stable metamaterial achieved good cushion performance by limiting the peak acceleration response through the peak force and trapping impact energy through the multi-stable mechanism.

CRediT authorship contribution statement

Xiao Ju: Writing – original draft, Visualization, Validation, Methodology, Investigation, Formal analysis, Data curation. **Shaoqi Li:** Writing – review & editing, Validation, Supervision, Project administration, Methodology, Conceptualization. **Yu Zhang:** Visualization, Investigation. **Penghao Wu:** Investigation, Data curation. **Yancheng Li:** Writing – review & editing, Supervision, Resources, Project administration, Funding acquisition.

Declaration of competing interest

The authors declare that they have no known competing financial interests or personal relationships that could have appeared to influence the work reported in this paper.

Data availability

Data will be made available on request.

Supplementary materials

Supplementary material associated with this article can be found, in the online version, at doi:10.1016/j.tws.2024.112120.

References

[1] D. Mu, H. Shu, L. Zhao, S. An, A review of research on seismic metamaterials, Adv. Eng. Mater. 22 (4) (2020) 1901148.
[2] T. Bückmann, M. Thiel, M. Kadic, R. Schittny, M. Wegener, An elasto-mechanical unfeelability cloak made of pentamode metamaterials, Nat. Commun. 5 (1) (2014) 4130.
[3] N. Li, S.Z. Liu, X.N. Wu, J.Y. Wang, Y.S. Han, X.C. Zhang, Mechanical characteristics of a novel rotating star-rhombic auxetic structure with multi-plateau stages, Thin Walled Struct. 191 (2023) 111081.
[4] L. Mizzi, L. Grasselli, A. Spaggiari, R. Gatt, P.S. Farrugia, J.N. Grima, Design of isotropic 2D chiral metamaterials based on monohedral pentagonal tessellations, Thin Walled Struct. 187 (2023) 110739.
[5] K. Li, Y. Zhang, Y. Hou, L. Su, G. Zeng, X. Xu, Mechanical properties of re-entrant anti-chiral auxetic metamaterial under the in-plane compression, Thin Walled Struct. 184 (2023) 110465.
[6] M. Gholikord, E. Etemadi, M. Imani, M. Hosseinabadi, H. Hu, Design and analysis of novel negative stiffness structures with significant energy absorption, Thin Walled Struct. 181 (2022).
[7] B. Chen, L. Chen, B. Du, H. Liu, W. Li, D. Fang, Novel multifunctional negative stiffness mechanical metamaterial structure: tailored functions of multi-stable and compressive mono-stable, Compos. Part B Eng. 204 (2021) 108501.
[8] S. Zhu, J. Wang, L. Chen, T. Liu, W. Li, Negative stiffness metamaterial with directional stability in uniform fields, Thin Walled Struct. 194 (2024) 111302.
[9] L.Y. Zhang, G.K. Xu, Negative stiffness behaviors emerging in elastic instabilities of prismatic tensegrities under torsional loading, Int. J. Mech. Sci. 103 (2015) 189–198.
[10] Y. Li, Z. Deng, G. Yan, G. Gao, Wave propagation in two-dimensional elastic metastructures with triangular configuration, Thin Walled Struct. 181 (2022) 110043.

[11] S. Guo, R. Gao, X. Tian, S.J. Liu, A quasi-zero-stiffness elastic metamaterial for energy absorption and shock attenuation, Eng. Struct. 280 (2023) 115687.
[12] H. Ma, K. Wang, H. Zhao, W. Shi, J. Xue, Y. Zhou, Q. Li, G. Wang, B. Yan, Energy dissipation and shock isolation using novel metamaterials, Int. J. Mech. Sci. 228 (2022) 107464.
[13] Z. Wang, X. Cao, H. Yang, X. Du, B. Ma, Q. Zheng, Z. Wan, Y. Li, Additively-manufactured 3D truss-lattice materials for enhanced mechanical performance and tunable anisotropy: simulations & experiments, Thin Walled Struct. 183 (2023) 110439.
[14] H. Jiang, B.A. Bednarcyk, L.L. Barbenchon, Y. Chen, Elastically anisotropic architected metamaterials with enhanced energy absorption, Thin Walled Struct. 192 (2023) 111115.
[15] S. Guo, R. Gao, X. Tian, S. Liu, A 3D metamaterial with negative stiffness for six-directional energy absorption and cushioning, Thin Walled Struct. 180 (2022) 109963.
[16] S. Chen, X. Tan, J. Hu, S. Zhu, B. Wang, L. Wang, Y. Jin, L. Wu, A novel gradient negative stiffness honeycomb for recoverable energy absorption, Compos. Part B Eng. 215 (2021) 108745.
[17] J. Zhou, H. Pan, C. Cai, D. Xu, Tunable ultralow frequency wave attenuations in one-dimensional quasi-zero-stiffness metamaterial, Int. J. Mech. Mater. Des. 17 (2021) 285–300.
[18] M. Zhang, C. Hu, C. Yin, Q.H. Qin, J. Wang, Design of elastic metamaterials with ultra-wide low-frequency stopbands via quantitative local resonance analysis, Thin Walled Struct. 165 (2021) 107969.
[19] R. Gao, S. Guo, X. Tian, S. Liu, A negative-stiffness based 1D metamaterial for bidirectional buffering and energy absorption with state recoverable characteristic, Thin Walled Struct. 169 (2021) 108319.
[20] Z. Cui, J. Qi, Y. Tie, T. Zou, Y. Duan, Research on the energy absorption properties of origami-based honeycombs, Thin Walled Struct. 184 (2023) 110520.
[21] B. Haghpanah, L. Salari-Sharif, P. Pourrajab, J. Hopkins, L. Valdevit, Multistable shape-reconfigurable architected materials, Adv. Mater. 28 (36) (2016) 7915–7920.
[22] S. Shan, S.H. Kang, J.R. Raney, P. Wang, L. Fang, F. Candido, J.A. Lewis, K. Bertoldi, Multistable architected materials for trapping elastic strain energy, Adv. Mater. 27 (29) (2015) 4296–4301.
[23] N. Hu, R. Burgueño, Buckling-induced smart applications: recent advances and trends, Smart Mater. Struct. 24 (6) (2015) 063001.
[24] S. Fang, S. Zhou, D. Yurchenko, T. Yang, W.H. Liao, Multistability phenomenon in signal processing, energy harvesting, composite structures, and metamaterials: a review, Mech. Syst. Signal Process. 166 (2022) 108419.
[25] H. Ma, K. Wang, H. Zhao, Y. Hong, Y. Zhou, J. Xue, Q. Li, G. Wang, B. Yan, Energy dissipation in multistable auxetic mechanical metamaterials, Compos. Struct. 304 (2023) 116410.
[26] J. Qiu, J.H. Lang, A.H. Slocum, A curved-beam bistable mechanism, J. Microelectromech. Syst. 13 (2) (2004) 137–146.
[27] S.A. Emam, D. Inman, A review on bistable composite laminates for morphing and energy harvesting, Appl. Mech. Rev. 67 (6) (2015) 060803.
[28] J. Hua, Y. Zhou, C.Q. Chen, Design and analysis of a tunable multistable mechanical metamaterial, Int. J. Mech. Sci. 272 (2024) 109170.
[29] R. Gao, M. Li, Q. Wang, J. Zhao, S.J. Liu, A novel design method of bistable structures with required snap-through properties, Sens. Actuators A Phys. 272 (2018) 295–300.
[30] Q. Luo, L. Tong, Optimal design of Bi-and multi-stable compliant cellular structures, in: Proceedings of the International Design Engineering Technical Conferences and Computers and Information in Engineering Conference, American Society of Mechanical Engineers, 2018. V05AT07A009.
[31] S. Guo, S. Liu, R. Gao, A bidirectional quasi-zero stiffness metamaterial for impact attenuation, Int. J. Mech. Sci. 268 (2024) 108998.
[32] Y. Zhang, M. Tichem, F. van Keulen, A novel design of multi-stable metastructures for energy dissipation, Mater. Des. 212 (2021) 110234.
[33] J.X. Wang, X. Liu, Q.S. Yang, R. Tao, Y. Li, L.H. Ma, A novel programmable composite metamaterial with tunable Poisson's ratio and bandgap based on multi-stable switching, Compos. Sci. Technol. 219 (2022) 109245.
[34] K. Liang, Y. Wang, Y. Luo, A. Takezawa, X. Zhang, Z. Kang, Programmable and multistable metamaterials made of precisely tailored bistable cells, Mater. Des. 227 (2023) 111810.
[35] D.M. Correa, T. Klatt, S. Cortes, M. Haberman, D. Kovar, C. Seepersad, Negative stiffness honeycombs for recoverable shock isolation, Rapid Prototyp. J. 21 (2) (2015) 193–200.
[36] X. Tan, B. Wang, S. Chen, S. Zhu, Y. Sun, A novel cylindrical negative stiffness structure for shock isolation, Compos. Struct. 214 (2019) 397–405.
[37] B. Wang, X. Tan, S. Zhu, S. Chen, K. Yao, P. Xu, L. Wang, H. Wu, Y. Sun, Cushion performance of cylindrical negative stiffness structures: analysis and optimization, Compos. Struct. 227 (2019) 111276.